ADVANCED OPTICAL MATERIALS
www.advopticalmat.de

Heterofission Mechanism for Pure Organic Room Temperature Phosphorescence

*Qi Sun, Jiajun Ren, Qian Peng, and Zhigang Shuai**

Room temperature phosphorescence (RTP) from pure organic materials, whether in crystalline or film phases, has recently attracted considerable attention. Experimental evidence increasingly suggests that RTP originates from isomeric dopants (impurity) rather than pure compounds. The underlying mechanism and molecular design principles have remained elusive. Herein, the "heterofission mechanism" for RTP is proposed, wherein a singlet excited state is split into two triplets, one remains within the host, while the other migrates to the guest (dopant) molecule, satisfying $E_{host}(S_1) \approx E_{host}(T_1) + E_{guest}(T_1)$. It is found that all the dopants possess a low triplet excited state, meeting the energy requirement for the heterofission process. The sum of the calculated emission spectra from these two triplets overlaps well with the experimentally measured broad phosphorescent spectra. Furthermore, the calculated heterofission rates are expected to occur at the picosecond timescale. Efficient Dexter energy transfer leads to the guest predominantly dominating the RTP. Based on this mechanism, we can predict potential host and guest candidates to expand the family of pure organic RTP materials.

1. Introduction

Organic functional materials, known for their easy processability, cost-effectiveness, and tunable colors, often exhibit intriguing properties such as room temperature phosphorescence (RTP).[1–7] Achieving several seconds of afterglow in RTP from pure organic materials is a remarkable accomplishment, particularly given the absence of metallic or inorganic elements.[8] Pure organic materials usually exhibit small spin-orbit coupling (SOC), which makes it difficult to give rise to RTP. However, significant progress has been made in recent years in achieving RTP in the crystalline or film form of pure organic systems, including carbazole (Cz), dibenzothiophene (DBT), fluorene, dibenzofuran, and others.[4,6,9–11] Host–guest systems for RTP materials have also been extensively explored.[4,6,9–11] Numerous strategies have been developed to achieve both high-efficiency and long lifetime RTP materials, including polymer dopant,[12] regulating aggregation morphology,[13–16] H-aggregation,[8] halogen bonding,[17,18] and so on. These strategies are designed to restrict intramolecular motion, thereby suppressing non-radiative decay processes and allowing for phosphorescent emission. Additionally, the crystalline environment and rigid molecular structures can hinder vibration-induced distortions to some extent, further limiting non-radiative decay and contributing to the achievement of long-lasting phosphorescence. The roles of intermolecular interaction (hydrogen bonding, π-halogen bonding, anion-π, and d-pπ bonds, and so forth) as well as the excited state compositions involving $\pi - \pi^*$ and $n - \pi^*$ components, have been found to be essential for understanding the intersystem crossing (ISC) process in RTP materials.[2,19]

It is worth noting that in metal-containing inorganic compounds, the ultralong afterglow is generally induced by impurity doping.[20,21] The photophysical properties of the same pure organic RTP materials measured by different research groups show considerable inconsistency,[5,11,22–24] such as BCZBP with 2.5% and 5.0% photoluminescence quantum yield (PLQY) and 0.11 ms and 0.28 s lifetime measured by two different groups,[23,24] respectively. These discrepancies have contributed to the ongoing debate and the perceived obscurity surrounding the mechanism of RTP in pure organic materials. Recently, Liu and coworkers raised the point that the lab-synthesized pure Cz, DBT, and their derivatives do not possess RTP properties. These authors have further applied high-performance liquid chromatography

Q. Sun, Z. Shuai
MOE Key Laboratory of Organic Optoelectronics and Molecular Engineering
Department of Chemistry
Tsinghua University
Beijing 100084, P. R. China
E-mail: ZGSHUAI@TSINGHUA.EDU.CN

J. Ren
MOE Key Laboratory of Theoretical and Computational Photochemistry
College of Chemistry
Beijing Normal University
Beijing 100875, P. R. China

Q. Peng
School of Chemical Sciences
University of Chinese Academy of Sciences
Beijing 100049, P. R. China

Z. Shuai
School of Science and Engineering
The Chinese University of Hong Kong
Shenzhen, Guangdong 518172, P. R. China

The ORCID identification number(s) for the author(s) of this article can be found under https://doi.org/10.1002/adom.202301769

DOI: 10.1002/adom.202301769

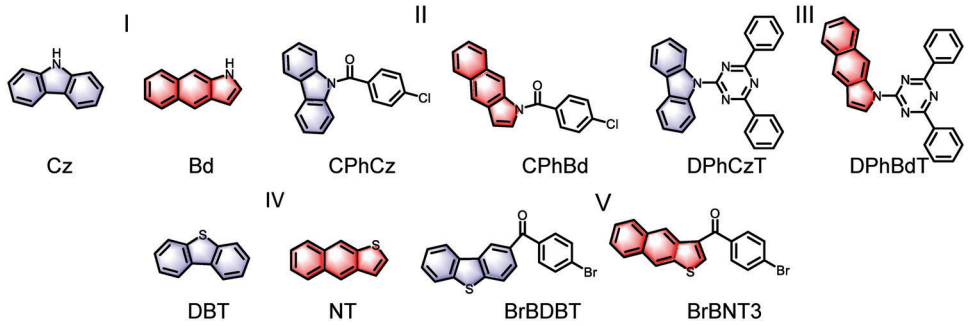

Figure 1. Chemical structures of the investigated materials. Molecules in blue are high T_1 moieties as host and molecules in red are low T_1 moieties as guest.

(HPLC) to successfully extract extremely small amounts of isomeric impurities, such as 1H-benzo[f]indole (Bd) from the commercial Cz product. They indicated that ultralong phosphorescence can be recovered by only 0.01 mol% Bd dopant in Cz.[25] In addition to Cz doped with Bd, other host/guest systems, such as CPhCz/CPhBd, DPhCzT/DPhBdT, DBT/NT, and BrBDBT/BrBNT3 (**Figure 1**), have been explored to demonstrate ultralong RTP,[25,26] providing substantial evidence for the effectiveness of the dopant strategy.[25,26] Regarding the mechanism, Liu and coworkers attributed the long-lived excitons to radical ions (Cz^-Bd^+ etc.) using the transient absorption spectra,[25,26] as these RTP materials have the same excited state absorption peaks (460–475 nm) as the reported donor (TMB) and acceptor (PPT) blend.[27] However, we contend that even when intermolecular radical ions form, the positions of the excited state absorption peaks for different ionic pairs may not necessarily be identical. Moreover, long-lived excitons are more likely to originate from triplet excitons. The reported theoretical calculations regarding fast charge transfer rate ($Cz^- + Cz = Cz + Cz^-$) and low Cz^-Bd^+ energy compared to Cz^-CZ^+ are also insufficient to confirm the formation of ionic pairs,[28] as it needs at least three steps, each with its own rate.

In contrast, our proposed mechanism suggests that heterofission processe results in the ultrafast formation of triplet excitons, with intermolecular charge transfer states (ICT) serving as virtual intermediate states. RTP originates from these heterofissioned triplet pairs. Heterofission, a special kind of singlet fission, entails the distribution of excitation energy from one chromophore in the excited singlet state to different chromophores, ultimately converting both into triplet states. Singlet fission processes have been used to generate double electron–hole pairs, which can enhance the efficiency of solar cells.[29,30] This process has also been used to generate double–triplet exciton and transfer its energy to phosphorencence materials via Dexter energy transfer, potentially leading to a breakthrough in the exciton utilization.[31,32] While the singlet fission process has been extensively studied, the fission process induced room temperature phosphorescence (RTP) is reported here for the first time, offering a fresh perspective on both singlet fission and RTP. Based on this mechanism, we can propose a molecular design strategy for RTP by identifying potential pure organic host and guest candidates through theoretical calculations.

2. Results and Discussion

2.1. Low T_1 Energy in the Dopants

In our computational approach for molecular geometry optimization and excited state calculations, we consider the donor–acceptor form of the host/guest dimers (CPhCz/CPhBd, DPhCzT/DPhBdT, and BrBDBT/BrBNT3). To this end, we employ the optimally tuned ωB97X-D (ωB97X-D*) functional coupled with the 6-31G* basis set. The triplet and singlet excitation energies, based on the T_1 optimized geometry of the investigated molecules, are shown in **Figure 2** and **Table 1**. It is important to emphasize that the lowest triplet state T_1 energy (1.49–1.74 eV) of the dopants (Bd, CPhBd, DPhBdT, NT, and BrBNT3) consistently remains quite low, much lower than that of the corresponding host materials (2.37–2.56 eV in Cz, CPhCz, DPhCzT, DBT, and BrBDBT). Such observations remind us that the low T_1 might be the primary reason for dopant-induced RTP. Notably, we observe that $E_{host}(S_1) \approx E_{host}(T_1) + E_{guest}(T_1)$, especially for the prototype RTP compound carbazole, that is, $E_{Cz}(S_1) > E_{Cz}(T_1) + E_{Bd}(T_1)$. This energy condition aligns with the requirements of the heterofission process.[29,33–35] Singlet fission process cannot be undergone for the pure host compound as the energy levels mismatch (Table 1). The value of $E_{host}(S_1) - E_{host}(T_1) - E_{guest}(T_1)$ in DPhCzT/DPhBdT is slightly negative (−0.2 eV), allowing for heterofission through an endothermic process. Heterofission, characterized by its spin-conserving nature, typically unfolds on the timescale of femtoseconds to picoseconds, making it ultrafast and capable of outcompeting other relaxation processes such as radiative and non-radiative decay, intersystem crossing (ISC), and so forth. The one with higher T_1 energy is denoted as host (Cz, CPhCz, DPhCzT, DBT, and BrBDBT in Figure 1), and the other one with lower triplet energy is guest (Bd, CPhBd, DPhBdT, NT, and BrBNT3).

2.2. Heterofission Induced the Formation of Triplet Exciton

To validate the hypothesis of the heterofission mechanism, we have computed the phosphorescence spectra of both the host and guest materials via the thermal vibration correlation function (TVCF) method implemented in our home-built MOMAP package[36–38] as shown in **Figure 3**. Across all five groups investigated here, the superposition of the calculated phosphorescence spectra from host and guest materials matches very well with ex-

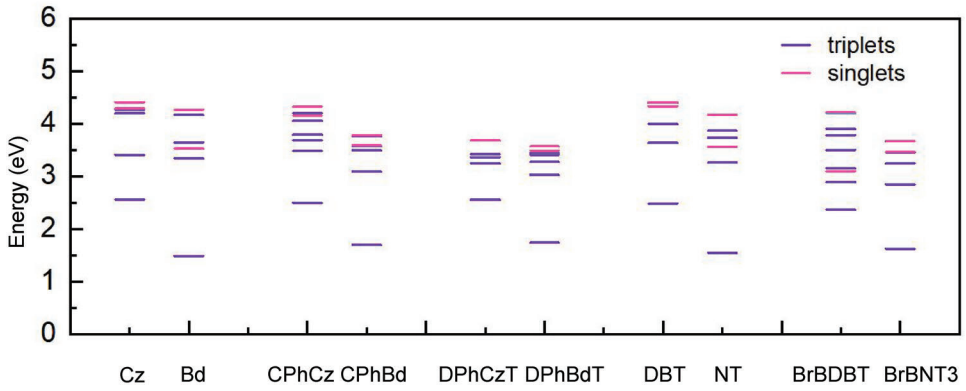

Figure 2. Excited state energies based on the optimized T_1 geometry of the investigated materials at the level of ωB97X-D*/6-31G(d).

perimental ones, confirming the formation of both triplet exciton from host and guest materials in experiments. The dominant spectral features are attributed to the longer wavelengths, which stem from the low T_1 energy of the guest materials. In contrast, the high T_1 energy of the host materials contributes less intensity to the shorter wavelengths. The currently calculated T_1 energies (1.49–1.74 eV) are based on the T_1 geometry, representing the vertical emission energy. Given that the phosphoresce spectra of the guest are broad (550–750 nm), it is difficult to obtain the vertical emission energy of the T_1 state in the experiment. Only the value of 0–0 transition energy of T_1 state could be approximately obtained in the experiment. Since all the essential information is encapsulated within the spectra, we consider the spectral comparison to be sufficient. The 0–0 transition energy corresponds to the adiabatic energy, the calculated 0–0 transition energy values are in the range of 2.39–2.47 eV (Table S1, Supporting Information), in excellent agreement with the experiment results. From our computed phosphorescence spectra, it is evident that both the peak positions and shapes align exceptionally well with the experimental results. The larger energy differences in excited states among different configurations are attributed to the significant reorganization energy within the systems. This reorgani-

Table 1. Energy difference between the host singlet state and its twice triplet state or the sum of triplet state energy of host and guest (Unit: eV).

Host/Guest	$E_{host}(S_1)$-$2E_{host}(T_1)$	$E_{host}(S_1)$-$E_{host}(T_1)$-$E_{guest}(T_1)$
Cz/Bd	−0.59	0.34
CPhCz/CPhBd	−0.69	0.06
DPhCzT/DPhBdT[a)]	−1.01	−0.2
DBT/NT	−0.64	0.3
BrBDBT/BrBNT3[a)]	−0.53	0.21

[a)] The second singlet excited energy is used in these system because of relatively large gaps between S_1 and S_2.

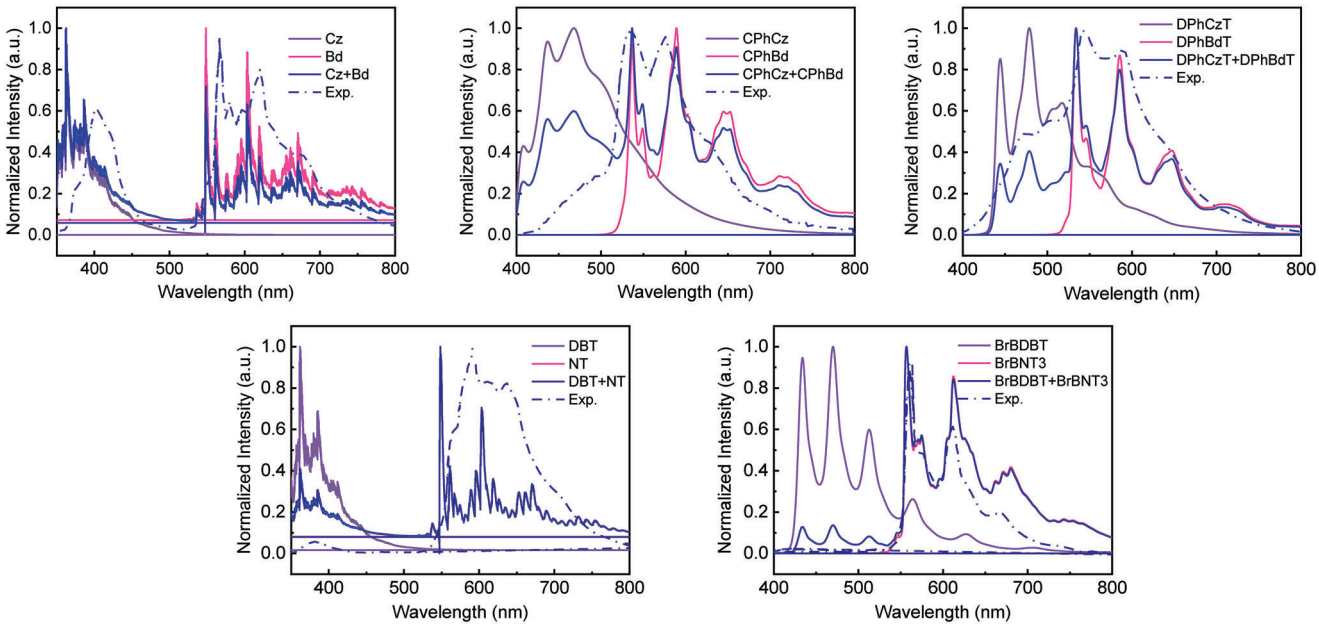

Figure 3. Theoretical calculations of the phosphorescence spectra and the comparison with the experimental ones (0.5 mol% guest doped in 99.5 mol% host). Reproduced with permission.[25] Copyright 2021, Springer Nature. Reproduced with permission.[26] Copyright 2022, John Wiley and Sons.

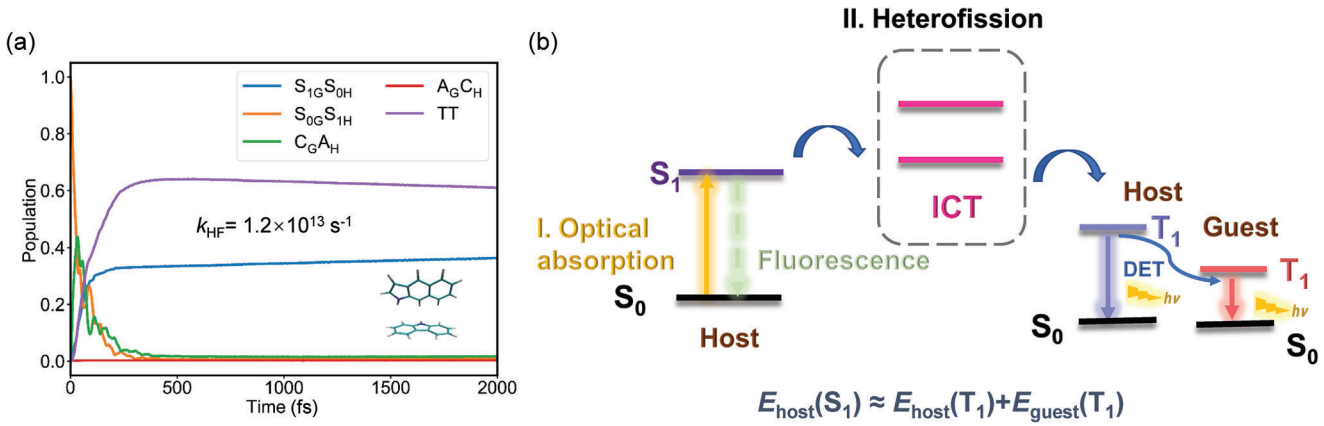

Figure 4. a) Population dynamics of heterofission process in the selected dimer (G: guest; H: host). b) Schematic diagram of the heterofission induced RTP mechanism. DET: Dexter energy transfer.

zation energy primarily arises from the stretching and bending vibrational modes of the fused molecular framework. For example, the total reorganization energy of the T_1 state for Cz and Bd on the S_0 (T_1) potential energy surface is 4390 cm^{-1} (4281 cm^{-1}) and 3388 cm^{-1} (3133 cm^{-1}), respectively. The most significant contribution to this is the stretching vibration of the condensed ring skeleton of Cz and Bd. The corresponding normal mode frequencies for this mode on the S_0 potential energy surface are 1723.62 and 1669.93 cm^{-1}, respectively, with a respective contribution of 2266.01 and 1569.27 cm^{-1} to the reorganization energy (Figure S1, Supporting Information). This characteristic leads to a broader phosphorescence spectrum, where the guest contribution in the spectra is distributed within the range of 550–800 nm.

The calculated shapes and positions of the spectral peaks closely resemble those observed in the experimental spectra, with the only difference being the presence of additional vibrational fine structures in the calculated spectra. This disparity is reasonable, as practical measurements are subject to various factors that can induce spectral broadening, thereby obscuring the vibrational fine structures in the experimental spectra. Furthermore, certain experimental evidence substantiates the occurrence of triplet exciton formation from both host and guest materials and the heterofission process: i) The experimental emission spectra at 77K for the mixture of BrBDBT and BrBNT3 show the superposition of those of BrBDBT and BrBNT3;[26] ii) BrBNT3 exhibit the lowest T_1 value, as observed from the 77K phosphorescence spectra, and perform best as the dopant;[26] iii) An optimal doping percentage, which is relatively low,[25,26] is imperative for the heterofission process. This necessity arises from the requirement that the ground state of the guest and the singlet exciton of the host engage in the heterofission process. A high guest concentration would lead to the formation of singlet exciton in the guest, and facilitating an effective energy transfer from the host to the guest, which is detrimental to the heterofission process. iv) The dopant is not necessarily an isomer of the host. For instance, Bd/CPhCz, Bd/DPhCzT, Cz/CPhBd, and Cz/DPhBdT have been demonstrated to exhibit RTP phenomena.[25]

The ICT state is generally viewed as an essential intermediate state to achieve ultrafast singlet fission dynamics.[39,40] Here we take the Cz/Bd dimer as an example to investigate the heterofission process. The crystals of Cz and Bd are both herringbone stacking, where the face-to-edge dimer is the pair with the shortest centroid distance. There are eight different stacking packing patterns all with the shortest contact for the hetero-dimer of Cz/Bd (**Figure 4**a; Figure S1, Supporting Information). In our approach, we replace one Cz with Bd in a 5 × 5 × 3 Cz cluster and adjust the orientation of Cz and Bd to create eight initial structures. Subsequently, we perform molecular mechanics optimization. Further details regarding the construction of the model Hamiltonian and the application of the time-dependent density-matrix renormalization group (TD-DMRG) method[41–43] for heterofission dynamics simulation are provided in the Experimental Section. Upon analyzing the population of the five involved lowest-lying states (Figure 4a; Figure S2, Supporting Information), it is found that the singlet exciton of the host Cz rapidly decays along with the generation of charge transfer states (especially the face part with negative charge and edge part with positive charge pairs with lower energy level),[44] the singlet exciton of guest Bd, and the TT state. One low-lying CT state exhibits a significant population, primarily attributed to the sequential CT-mediated regime. The other CT state with higher energy is not directly populated, as it is associated with the superexchange CT-mediated regime. Both of these regimes contribute to ultrafast heterofission dynamics.[39] It is important to note that the formation of the guest singlet exciton competes with the heterofission process, underscoring the need for a low dopant concentration to prevent energy transfer from the host singlet exciton to the guest materials. The heterofission rate ($1/\tau$) can be fitted from the TT state population ($p(t)$) using $p(t) = a - b\exp(-t/\tau)$ (t: time), the fitting rate (k_{HF}) is 1.2 × 10^{13} s^{-1}, manifesting an ultrafast process that could outcompete other relaxation processes. The TT population is the dominant component, resulting in a significant triplet yield.

Once the triplet excitons of host and guest are formed, efficient Dexter energy transfer from host to guest becomes possible. We determined the triplet energy transfer rate (k_{DET}) by employing Fermi's Golden Rule (FGR), considering the quantum nature of all the molecular vibrational modes. Under strong coupling and high temperature approximation, this formalism converges to the semiclassical Marcus theory. For the selected Cz/Bd pair, the Dexter energy transfer rate is calculated to be 3.71 × ˜10^5˜s^{-1} with FGR and 6.81 × ˜10^5˜s^{-1} with

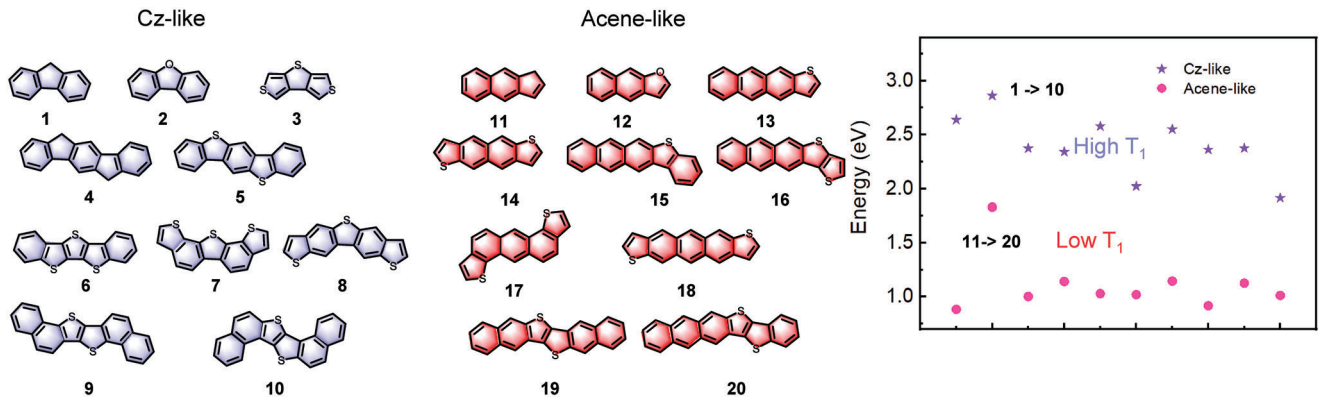

Figure 5. Candidates as host materials (blue) and guest molecules (red) and their T_1 energy of optimized T_1 geometry calculated at the level of ωB97X-D/6-31G(d).

semiclassical Marcus theory, respectively. As a result, the guest molecule predominantly influences RTP, leading to intense emission at longer wavelengths. The overall process of intermolecular charge transfer-mediated heterofission inducing RTP can be illustrated as shown in Figure 4b: i) Initially, the singlet exciton of the host materials (S_{1H}) is populated (host material is the dominant component), likely resulting in prompt fluorescence (corresponding to the prompt part of the experimental spectra[25,26]). ii) Combined with ground state guest (S_{0G}), using ICT as intermediate states, the heterofission process occurs, leading to the formation of triplet excitons of host and guest. iii) Dexter energy transfer (DET) occurs from host to guest, the triplet exciton of host and guest decays to the ground state and emits RTP.

2.3. Nature of Triplet States

To get a deep insight into the structure–property relationship, we analyze the T_1 transition properties of these molecules as depicted in Figure S3, Supporting Information. They are all in a locally excited (LE) dominant state, with transition density concentrated on the Cz or Bd or DBT or NT moiety. Consequently, the high T_1 state in Cz derivatives (CPhCz and DPhCzT) and DBT derivative (BrBDBT) are maintained, and the low T_1 state in Bd derivatives (CPhBd and DPhBdT) and NT derivative (BrBNT3) are conserved. In terms of frontier orbitals, the high T_1 moiety hosts Cz and DBT show similar frontier orbital nodes, which we denote as Cz-like, while the low T_1 moiety guests Bd and NT show the acence-like frontier orbital nodes. This disparity leads to the notable difference in T_1 energy levels. To provide further insight, we plot the iso-chemical-shielding surfaces (ICSS)[45,46] of Cz, Bd, DBT, and NT in Figure S4, Supporting Information. It is evident that Bd and NT exhibit higher aromaticity, which subsequently results in lower T_1 energy levels. Additionally, we conducted calculations for the CPhCz and CPhBd dimers to consider intermolecular interactions. As indicated in the results presented in Figure S5, Supporting Information, no ICT state is formed, and the T_1 state of such a dimer remains localized on the low T_1 moiety, Bd. This observation aligns with our previous work, where it was demonstrated that the low T_1 state is maintained when connected with other high T_1 moieties.[31]

2.4. Providing Host and Guest Candidates

To expand the range of possible RTP candidates, we aim to align the characteristics of the host and guest units. Specifically, we seek host units with high T_1 possessing Cz-like frontier orbital nodes and guest moieties with low T_1 exhibiting acene-like frontier orbital nodes. This strategy allows us to diversify the family of RTP candidates, as depicted in **Figure 5**. All the molecules consist of fused rings, similar to Cz, Bd, DBT, and NT, making them suitable as fundamental building blocks for various derivatives. In fact, molecules 1–20 have already been synthesized in experiments. These compounds typically serve as fundamental units in luminescent and transport materials, with some displaying the potential for high luminescence and mobility simultaneously.[47] Notably, molecules 1–10, characterized by Cz-like frontier orbital nodes (as shown in Figure S6, Supporting Information), exhibit higher T_1 values than molecules 11–20, which feature acene-like frontier orbital nodes (Figure S6, Supporting Information). This observation aligns with our previous discussion and confirms the effectiveness of our design strategy. Traditionally, the design of singlet fission materials has relied solely on energy alignment based on theoretical calculations.[48,49] The value of $E_{host}(S_1) - E_{host}(T_1) - E_{guest}(T_1)$ in these host/guest systems is calculated in **Table 2** and Tables S4–S5, Supporting Information, with positive values observed in all cases except for compound 12 as guest, which displays slightly negative values. This trend indicates the effectiveness of utilizing Cz-like frontier orbital nodes as the core moiety in host materials and acene-like frontier orbital nodes as the unit in guest materials. Additionally, compounds 11–20 have also been treated as host materials, and the corresponding values of $E_{host}(S_1) - E_{host}(T_1) - E_{guest}(T_1)$ are listed in Tables S4 and S5, Supporting Information, to assess their suitability as hosts. This approach opens up the possibility of generating numerous derivatives using 1–20 as the core. Besides, other low T_1 moiety, such as partial conjugated five-membered rings[31] may also be useful if the $E_{host}(S_1) \approx E_{host}(T_1) + E_{guest}(T_1)$ is satisfied.

3. Conclusion

In conclusion, we propose the heterofission mechanism to explain the dopant-induced RTP of pure organic materials by

Table 2. $E_{host}(S_1)$-$E_{host}(T_1)$-$E_{guest}(T_1)$ values in host/guest system, 1–10 are host materials and 11–20 with lower $E(T_1)$ are guest (Unit: eV).

Host/Guest	11	12	13	14	15	16	17	18	19	20
1	0.94	0.00	0.82	0.69	0.80	0.81	0.68	0.91	0.70	0.81
2	0.89	−0.05	0.77	0.64	0.75	0.76	0.63	0.86	0.65	0.76
3	1.20	0.25	1.08	0.94	1.05	1.06	0.94	1.16	0.96	1.07
4	0.63	−0.31	0.51	0.38	0.49	0.50	0.37	0.60	0.39	0.50
5	0.48	−0.47	0.36	0.22	0.33	0.34	0.21	0.44	0.23	0.35
6	0.67	−0.28	0.55	0.41	0.52	0.53	0.41	0.63	0.42	0.54
7	0.46	−0.49	0.34	0.20	0.31	0.32	0.20	0.42	0.22	0.33
8	0.64	−0.31	0.52	0.38	0.49	0.50	0.38	0.60	0.39	0.51
9	0.45	−0.49	0.33	0.19	0.31	0.32	0.19	0.42	0.21	0.32
10	0.55	−0.39	0.43	0.29	0.41	0.41	0.29	0.52	0.31	0.42

means of quantum chemistry calculations and quantum dynamics simulation. A singlet excited state in the host molecule can split into two triplets, with one in the host and the other in the guest. The latter possesses a much lower triplet state than the former. This unique mechanism offers a rational approach to designing organic RTP materials. The prerequisite lies in the low T_1 nature of the dopants, which triggers the heterofission process, resulting in the rapid formation of triplet excitons. It is found that the experimental phosphorescence spectra for a number of RTP systems can be well fit by the superposition of the calculated triplet emission spectra from host and guest molecules. Quantum dynamics simulations, employing the TD-DMRG method with a model Hamiltonian derived from the host-guest dimer formed in the crystalline structure, consistently support the dominance of the heterofission process. Additionally, efficient Dexter energy transfer contributes to the intense emission of the guest molecule at longer wavelengths. Ultimately, our research extends the possibilities of pure organic RTP systems by presenting potential candidate molecules for further exploration. This study not only provides a novel understanding of the mechanism behind dopant-induced RTP in pure organic materials but also offers valuable guidelines for the design of RTP materials.

4. Experimental Section

Ground state S_0, excited state S_1, T_1 geometry optimization, and corresponding frequency vibrations along with the excitation energies, were calculated at the level of optimal tuned ωB97X-D (ωB97X-D*) functional with a 6-31G* basis in Gaussian 16 package.[50] An optimally tuned ω value in a range-separated functional like ωB97X-D is an accurate and efficient way to calculate the charge transfer state, which has received widespread recognition.[51–53] The basis is Koopman's Theorem, that is, the calculated ionization potential is equal to the calculated negative value of the HOMO energy. The ω values of the investigated system are shown in Table S2, Supporting Information. Geometry optimization, frequency calculation, and excitation energy were all conducted in the vacuum environment, as the exciton coupling and transfer integral were small in a system like this as reported in the literature.[47] According to the TVCF method,[36–38] the phosphorescence emission cross section σ_{em} could be written as:

$$\sigma_{em}(\omega) = \frac{2\omega^3}{3\pi\hbar c^3}\|\mu_T\|^2 \int_{-\infty}^{+\infty} e^{-i(\omega-\omega_T)t}\rho_{em}(t, T)dt \quad (1)$$

where c is the speed of light, ω_T is the T_1 energy, μ_T is the transition dipole moment of T_1 state, $\rho_{em}(t, T)$ is the Franck–Condon overlap at temperature T. The relative intensities of the host/guest spectra were influenced by various factors during radiative and non-radiative processes; hence, these intensities are derived from experimentally measured relative intensities. Iso-chemical-shielding surfaces (ICSS) using the nucleus-independent chemical shift (NICS) concept were calculated at B3LYP/6-31+G* with the help of Multiwfn.[45,46] Herein, the $ICSS_{zz}(1)$ (the value of ICSS which is perpendicular to and 1 Å above the plane of the molecule) surfaces were employed instead of ICSS, as the $NICS_{zz}(1)$ performed better as an aromaticity judgment than NICS. The different color schemes were used to manifest different magnetic shielding isosurface values in ppm. The transition dipole moment of the T_1 state was carried out in Dalton.[54] The energy minimization process was performed with a general AMBER force field (GAFF) considering periodic boundary conditions (PBC) in the GROMACS 2019 package.[55]

Under Fermi's Golden Rule (FGR) regime, the quantum Dexter energy transfer rate could be expressed as:

$$k_{DET,FGR} = \frac{1}{\hbar^2}|V|^2 \int_{-\infty}^{\infty} dt \exp\{i\omega_{fi}t - \sum_j S_j[(2\bar{n}_j + 1) - \bar{n}_j e^{-i\omega_j t} - (\bar{n}_j + 1)e^{i\omega_j t}]\} \quad (2)$$

where V is the exchange integral between host and guest, ω_{fi} is the energy difference between host and guest, $n_j = \frac{1}{e^{\hbar\omega_j/k_B T}-1}$ is the population of the jth normal mode with frequency ω_j. S_j is the Huang–Rhys factor of the T_1 state. The semiclassical Marcus energy transfer rate is:

$$k_{DET,Marcus} = \frac{V^2}{\sqrt{\lambda k_B T/\pi}} \exp[-\frac{(\omega_{fi} + \lambda)^2}{4\lambda k_B T}] \quad (3)$$

λ is reorganization energy, which is expressed as $\sum_j \hbar\omega_j S_j$, namely, a sum of relaxation energy from all the normal modes. All the required parameters presented here are obtained through quantum chemistry calculations, which are then used as inputs to our home-built program MOMAP[36–38] to obtain the energy transfer rates.

To describe the heterofission dynamics, we first construct a vibronic Hamiltonian, which could be written as:

$$\hat{H} = \hat{H}_e + \hat{H}_{ph} + \hat{H}_{e-ph} \quad (4)$$

where $\hat{H}_{ph}$ and $\hat{H}_{e-ph}$ are phonon vibration and electron-vibration coupling, respectively. Modes with a Huang–Rhys factor ⩾0.01 were chosen here for simplifying the calculation. And $\hat{H}_e$ is pure electron Hamiltonian, which could be expressed in the five diabatic states $S_{1G}S_{0H}$, $S_{0G}S_{1H}$, C_GA_H, A_GC_H, and T_GT_H (C: cation; A: anion):

$$\hat{H}_e = \begin{bmatrix} E(S_{1G}S_{0H}) & J & V_{ll} & -V_{hh} & 0 \\ J & E(S_{0G}S_{1H}) & -V_{hh} & V_{ll} & 0 \\ V_{ll} & -V_{hh} & E(C_GA_H) & 0 & \sqrt{3/2}V_{lh} \\ -V_{hh} & V_{ll} & 0 & E(A_GC_H) & \sqrt{3/2}V_{hl} \\ 0 & 0 & \sqrt{3/2}V_{lh} & \sqrt{3/2}V_{hl} & E(T_GT_H) \end{bmatrix} \quad (5)$$

The diagonal elements are the on-site energy of the five states. And the off-diagonal parts are the couplings between them. The energy of the first four states and their couplings could be obtained using Boys localized diabatization[56] method built in Q-Chem package.[57] $E(T_GT_H)$ denotes the sum of the T_1 energy of the single molecule, and the couplings between the ICT state and the TT state were obtained through the PySCF package.[58] The results of the localized diabatic states in 8 group molecules and their corresponding matrix elements are shown in Figure S7, Supporting Information. The Bond dimension in the TD-DMRG simulation was set to 100, the singlet exciton of the host was chosen as

the initial state and the temperature was 300 K. All the TD-DMRG calculations were performed in the open-source package Renormalizer.[41–43] The dynamic behavior was determined by the electronic Hamiltonian Equation (5) as well as the vibronic component. Given that the packing geometry involving one host and one guest within the surplus host molecules (5 × 5 × 3) cluster was considered, the matrix elements of the electronic Hamiltonian were particularly influenced by the packing geometry. Once the packing geometry was established, vacuum or QM/MM calculations could yield similar behavior, consistent with previous research by the authors.[44] Regarding the vibronic component, since the phosphorescence spectra that were calculated closely match the experimental ones, it was believed that performing vibronic calculations in the vacuum phase is sufficient. Based on this mechanism, a computational formula for the phosphorescence luminescence efficiency (Φ_{PLQY}) of the host–guest doping system could be derived:

$$\Phi_{PLQY} = \Phi_{HF}[\frac{k_{rH}}{k_{rH}+k_{nrH}+k_{DET}} + \frac{k_{rG}}{k_{rG}+k_{nrG}} (1+\frac{k_{DET}}{k_{rH}+k_{nrH}+k_{DET}})] \quad (6)$$

where Φ_{HF} is the heterofission yield, k_{rH}, k_{rG}, k_{nrH}, and k_{nrG} denote the radiative rate (k_r) and non-radiative rate (k_{nr}) of host (H) and guest (G), respectively. k_{DET} is the Dexter energy transfer rate (from the host to the guest).

Supporting Information

Supporting Information is available from the Wiley Online Library or from the author.

Acknowledgements

This work was supported by the National Natural Science Foundation of China (Grant Nos. 21973099, 22273105, and 22273005) and by the Shenzhen Science and Technology Program.

Conflict of Interest

The authors declare no conflict of interest.

Data Availability Statement

The data that support the findings of this study are available from the corresponding author upon reasonable request.

Keywords

dopants, heterofission, molecular design, room temperature phosphorescence

Received: July 25, 2023
Revised: September 27, 2023
Published online: October 28, 2023

[1] Y. Li, M. Gecevicius, J. Qiu, *Chem. Soc. Rev.* **2016**, *45*, 2090.
[2] Q. Peng, H. Ma, Z. Shuai, *Acc. Chem. Res.* **2021**, *54*, 940.
[3] S. M. A. Fateminia, Z. Mao, S. Xu, Z. Yang, Z. Chi, B. Liu, *Angew. Chem., Int. Ed.* **2017**, *56*, 12160.
[4] W. Zhao, Z. He, J. W. Lam, Q. Peng, H. Ma, Z. Shuai, G. Bai, J. Hao, B. Tang, *Chem.* **2016**, *1*, 592.
[5] Y. Xie, Y. Ge, Q. Peng, C. Li, Q. Li, Z. Li, *Adv. Mater.* **2017**, *29*, 1606829.
[6] W. Zhao, T. S. Cheung, N. Jiang, W. Huang, J. W. Y. Lam, X. Zhang, Z. He, B. Z. Tang, *Nat. Commun.* **2019**, *10*, 1595.
[7] R. Liu, Y. Ge, D. Wang, Z. Shuai, *CCS Chem.* **2021**, *3*, 1477.
[8] Z. An, C. Zheng, Y. Tao, R. Chen, H. Shi, T. Chen, Z. Wang, H. Li, R. Deng, X. Liu, W. Huang, *Nat. Mater.* **2015**, *14*, 685.
[9] Kenry, C. Chen, B. Liu, *Nat. Commun.* **2019**, *10*, 2111.
[10] C. S. Bilen, N. Harrison, D. J. Morantz, *Nature* **1978**, *271*, 235.
[11] Y. Xiong, Z. Zhao, W. Zhao, H. Ma, Q. Peng, Z. He, X. Zhang, Y. Chen, X. He, J. W. Y. Lam, B. Z. Tang, *Angew. Chem., Int. Ed.* **2018**, *57*, 7997.
[12] G. Zhang, J. Chen, S. J. Payne, S. E. Kooi, J. N. Demas, C. L. Fraser, *J. Am. Chem. Soc.* **2007**, *129*, 8942.
[13] G. Bergamini, A. Fermi, C. Botta, U. Giovanella, S. Di Motta, F. Negri, R. Peresutti, M. Gingras, P. Ceroni, *J. Mater. Chem. C* **2013**, *1*, 2717.
[14] Y. Gong, L. Zhao, Q. Peng, D. Fan, W. Z. Yuan, Y. Zhang, B. Z. Tang, *Chem. Sci.* **2015**, *6*, 4438.
[15] C. Li, X. Tang, L. Zhang, C. Li, Z. Liu, Z. Bo, Y. Q. Dong, Y.-H. Tian, Y. Dong, B. Z. Tang, *Adv. Opt. Mater.* **2015**, *3*, 1184.
[16] W. Z. Yuan, X. Y. Shen, H. Zhao, J. W. Y. Lam, L. Tang, P. Lu, C. Wang, Y. Liu, Z. Wang, Q. Zheng, J. Z. Sun, Y. Ma, B. Z. Tang, *J. Phys. Chem. C* **2010**, *114*, 6090.
[17] O. Bolton, D. Lee, J. Jung, J. Kim, *Chem. Mater.* **2014**, *26*, 6644.
[18] O. Bolton, K. Lee, H.-J. Kim, K. Y. Lin, J. Kim, *Nat. Chem.* **2011**, *3*, 205.
[19] H. Ma, Q. Peng, Z. An, W. Huang, Z. Shuai, *J. Am. Chem. Soc.* **2019**, *141*, 1010.
[20] M. Lastusaari, T. Laamanen, M. Malkamäki, K. O. Eskola, A. Kotlov, S. Carlson, E. Welter, H. F. Brito, M. Bettinelli, H. Jungner, J. Hölsä, *Eur. J. Miner.* **2012**, *24*, 885.
[21] K. Van den Eeckhout, P. F. Smet, D. Poelman, *Materials* **2010**, *3*, 2536.
[22] S. Cai, H. Shi, J. Li, L. Gu, Y. Ni, Z. Cheng, S. Wang, W.-w. Xiong, L. Li, Z. An, W. Huang, *Adv. Mater.* **2017**, *29*, 1701244.
[23] Y. Gong, G. Chen, Q. Peng, W. Z. Yuan, Y. Xie, S. Li, Y. Zhang, B. Z. Tang, *Adv. Mater.* **2015**, *27*, 6195.
[24] Z. Yang, Z. Mao, X. Zhang, D. Ou, Y. Mu, Y. Zhang, C. Zhao, S. Liu, Z. Chi, J. Xu, Y.-C. Wu, P.-Y. Lu, A. Lien, M. R. Bryce, *Angew. Chem., Int. Ed.* **2016**, *55*, 2181.
[25] C. Chen, Z. Chi, K. C. Chong, A. S. Batsanov, Z. Yang, Z. Mao, Z. Yang, B. Liu, *Nat. Mater.* **2021**, *20*, 175.
[26] K. C. Chong, C. Chen, C. Zhou, X. Chen, D. Ma, G. C. Bazan, Z. Chi, B. Liu, *Adv. Mater.* **2022**, *34*, 2201569.
[27] R. Kabe, C. Adachi, *Nature* **2017**, *550*, 384.
[28] F. J. Hernández, R. Crespo-Otero, *J. Mater. Chem. C* **2021**, *9*, 11882.
[29] M. B. Smith, J. Michl, *Chem. Rev.* **2010**, *110*, 6891.
[30] M. B. Smith, J. Michl, *Annu. Rev. Phys. Chem.* **2013**, *64*, 361.
[31] Q. Sun, Y. Wu, Y. Cui, C. Gao, Q. Ou, D. Hu, L. Wang, Y. Wang, H. Dong, J. Zhao, C. Zhang, Z. Shuai, H. Fu, Q. Peng, *Mater. Horiz.* **2022**, *9*, 2518.
[32] R. Nagata, H. Nakanotani, W. J. Potscavage Jr, C. Adachi, *Adv. Mater.* **2018**, *30*, 1801484.
[33] K. von Burg, I. Zschokke-Gränacher, *J. Chem. Phys.* **1979**, *70*, 3807.
[34] N. Geacintov, J. Burgos, M. Pope, C. Strom, *Chem. Phys. Lett.* **1971**, *11*, 504.
[35] M. Charbr, D. Williams, *Chem. Phys. Lett.* **1977**, *49*, 599.
[36] Z. Shuai, Q. Peng, *Nat. Sci. Rev.* **2017**, *4*, 224.
[37] Q. Peng, Y. Yi, Z. Shuai, J. Shao, *J. Am. Chem. Soc.* **2007**, *129*, 9333.
[38] Z. Shuai, *Chin. J. Chem.* **2020**, *38*, 1223.
[39] T. C. Berkelbach, M. S. Hybertsen, D. R. Reichman, *J. Chem. Phys.* **2013**, *138*, 114102.
[40] T. C. Berkelbach, M. S. Hybertsen, D. R. Reichman, *J. Chem. Phys.* **2013**, *138*, 114103.

[41] J. Ren, Z. Shuai, G. Kin-Lic Chan, *J. Chem. Theory Comput.* **2018**, *14*, 5027.
[42] J. Ren, W. Li, T. Jiang, Y. Wang, Z. Shuai, *WIREs Comput. Mol. Sci.* **2022**, *12*, e1614.
[43] W. Li, J. Ren, Z. Shuai, *J. Chem. Phys.* **2020**, *152*, 024127.
[44] Q. Sun, J. Ren, T. Jiang, Q. Peng, Q. Ou, Z. Shuai, *Nano Lett.* **2021**, *21*, 5394.
[45] Z. Liu, T. Lu, Q. Chen, *Carbon* **2020**, *165*, 468.
[46] T. Lu, F. Chen, *J. Comput. Chem.* **2012**, *33*, 580.
[47] Q. Sun, T. Jiang, Q. Ou, Q. Peng, Z. Shuai, *Adv. Opt. Mater.* **2023**, *11*, 2202621.
[48] A. Akdag, Z. Havlas, J. Michl, *J. Am. Chem. Soc.* **2012**, *134*, 14624.
[49] Q. Li, Y.-H. Kan, H.-L. Xu, Z.-M. Su, *J. Am. Chem. Soc.* **2020**, *142*, 11791.
[50] M. J. Frisch, G. W. Trucks, H. B. Schlegel, G. E. Scuseria, M. A. Robb, J. R. Cheeseman, G. Scalmani, V. Barone, G. A. Petersson, H. Nakatsuji, X. Li, M. Caricato, A. V. Marenich, J. Bloino, B. G. Janesko, R. Gomperts, B. Mennucci, H. P. Hratchian, J. V. Ortiz, A. F. Izmaylov, J. L. Sonnenberg, D. Williams-Young, F. Ding, F. Lipparini, F. Egidi, J. Goings, B. Peng, A. Petrone, T. Henderson, D. Ranasinghe, et al., Gaussian 16 Revision B.01, Gaussian Inc., Wallingford, CT **2016**.
[51] T. Stein, L. Kronik, R. Baer, *J. Am. Chem. Soc.* **2009**, *131*, 2818.
[52] P. K. Samanta, D. Kim, V. Coropceanu, J.-L. Brédas, *J. Am. Chem. Soc.* **2017**, *139*, 4042.
[53] H. Sun, C. Zhong, J.-L. Brédas, *J. Chem. Theory Comput.* **2015**, *11*, 3851.
[54] K. Aidas, C. Angeli, K. L. Bak, V. Bakken, R. Bast, L. Boman, O. Christiansen, R. Cimiraglia, S. Coriani, P. Dahle, E. K. Dalskov, U. Ekström, T. Enevoldsen, J. J. Eriksen, P. Ettenhuber, B. Fernández, L. Ferrighi, H. Fliegl, L. Frediani, K. Hald, A. Halkier, C. Hättig, H. Heiberg, T. Helgaker, A. C. Hennum, H. Hettema, E. Hjertenæs, S. Høst, I.-M. Høyvik, M. F. Iozzi, *et al. WIREs Comput. Mol. Sci.* **2014**, *4*, 269.
[55] B. Hess, C. Kutzner, D. van der Spoel, E. Lindahl, *J. Chem. Theory Comput.* **2008**, *4*, 435.
[56] J. E. Subotnik, S. Yeganeh, R. J. Cave, M. A. Ratner, *J. Chem. Phys.* **2008**, *129*, 244101.
[57] Y. Shao, Z. Gan, E. Epifanovsky, A. T. Gilbert, M. Wormit, J. Kussmann, A. W. Lange, A. Behn, J. Deng, X. Feng, D. Ghosh, M. Goldey, P. R. Horn, L. D. Jacobson, I. Kaliman, R. Z. Khaliullin, T. Kuś, A. Landau, J. Liu, E. I. Proynov, Y. M. Rhee, R. M. Richard, M. A. Rohrdanz, R. P. Steele, E. J. Sundstrom, H. L. W. III, P. M. Zimmerman, D. Zuev, B. Albrecht, E. Alguire, *et al. Mol. Phys.* **2015**, *113*, 184.
[58] Q. Sun, T. C. Berkelbach, N. S. Blunt, G. H. Booth, S. Guo, Z. Li, J. Liu, J. D. McClain, E. R. Sayfutyarova, S. Sharma, S. Wouters, G. K.-L. Chan, *WIREs Comput. Mol. Sci.* **2018**, *8*, e1340.